The Scattering of Continental Shelf Waves by an Isolated Topographic Irregularity

SHENN-YU CHAO, LEONARD J. PIETRAFESA AND GERALD S. JANOWITZ

Department of Marine Science and Engineering, North Carolina State University, Raleigh 27650

(Manuscript received 31 August 1978, in final form 15 January 1979)

ABSTRACT

A model for the scattering of a continental shelf wave by a small, isolated and smooth topographic irregularity is developed. It is found that a wave of frequency ω, incident on a bump of a sufficiently small horizontal extent such that the solution for a delta-function bump will apply, will trigger all other allowable modes of the same frequency with the highest modes having the largest amplitudes. Further, the higher the mode of the incoming wave, the more strongly will it be scattered. Thus, for a continuous spectrum of continental shelf waves propagating over complicated and extended topography, one would expect a net cascading process toward the higher wavenumber end of the spectrum due solely to the effects of topography. It is noted, however, that if the solution is integrated over a bump of large horizontal extent, the behavior of the forward-scattered and backscattered waves could be entirely different from that of a delta function bump.

1. Introduction

The effect of topographic irregularities on the propagation of continental shelf waves (CSW's) has been of considerable recent interest. Allen (1976) investigated the effect of a longshore topographic irregularity on barotropic long CSW's by considering small variations in lateral and bottom topography. Buchwald (1977) addressed the problem of the diffraction of CSW's due to the presence of an irregular coastline; no longwave approximation was used in the model. Further, Odulo (1975) and Huthnance (1975) have shown that for a continental margin characterized by a bottom depth h, which varies only in the cross-shelf direction x, if the quantity h_x/h remains bounded, then the group velocities of all CSW modes can be both positive and negative. Moreover, the resultant dispersion relation indicates that both forward- and backward scattering of wave energy can occur whenever a CSW encounters a topographic irregularity.

The case of an extremum in the group velocity of CSW's can be characterized as an Airy phase (Lighthill, 1965). For the particular case of zero-group speed (ZGS) waves the Airy phase does not propagate, and LeBlond and Mysak (1977) suggest that there should then be enhanced amplified persistance of phenomena locally generated at the appropriate wavelengths. Buchwald's theoretical results essentially confirm LeBlond and Mysak's contention and observational evidence presented by Cutchin and Smith (1973) and Hamon (1976) seemingly lends support to the argument.

In this paper, we consider the effects of a small, smooth and isolated topographic irregularity on CSW propagation along a continental shelf, the depth of which increases exponentially in the offshore direction; no longwave approximation is invoked. In comparison to the cited work of Allen, this work considers the entire dispersion curve. Moreover, this effort examines the effects of a small, isolated topographic irregularity on the shelf proper, in deference to the referenced work of Buchwald, which assumes the coast to be irregular. Although this paper essentially deals with a topographic irregularity of small horizontal extent, the analysis can be extended to a bump of large horizontal extent by integrating our solution over the extended topography.

Section 2 provides the details of the mathematical formulation and the solution. Numerical results are given in Section 3, and a discussion of model results, as well as conclusions, are presented in Section 4.

2. Analysis

We consider a barotropic, essentially inviscid, coastal ocean on a constant f-plane of the Northern Hemisphere. The continental shelf zone is bounded on the west by a coast at $x' = 0$, and on the east at $x' = L$. The water depth beyond the shelf zone

0022-3670/79/040687-09$06.25

is a constant H_0. A rigid lid on the surface of the water extended from the coastline to the edge of the shelf is also assumed initially. Let f^{-1} be the time scale, H_0 the depth scale, L the horizontal length scale, and fL^2H_0 the streamfunction scale. The dimensionless, vertically integrated, linear vorticity equation and boundary conditions for the coastal trapped waves are (see, e.g., Allen, 1976; Buchwald, 1977)

$$\left.\begin{aligned} &\left(\Psi_{xx} + \Psi_{yy} - \frac{h_x}{h}\Psi_x - \frac{h_y}{h}\Psi_y\right)_t + \frac{h_x}{h}\Psi_y - \frac{h_y}{h}\Psi_x = 0, && x \leqslant 1 \\ &\Psi_{xx} + \Psi_{yy} - \beta^2\Psi = 0, && x \geqslant 1 \\ &\Psi(x = 0, y, t) = \Psi(x \to \infty, y, t) = 0, \end{aligned}\right\}, \tag{1}$$

where y is positive poleward, $h(x,y)$ is the water depth profile, and Ψ the mass transport streamfunction defined such that $hu = \Psi_y$ and $hv = -\Psi_x$ for velocity components (u,v) in the (x,y) directions. A small divergence parameter $\beta^2 = f^2/gH_0$ is used only for $x \geqslant 1$. The use of the small divergence parameter is conceptual and helps us to complete the contours of integration, as will be shown. Eventually the limit of $\beta^2 \to 0$ will be required and a rigid-lid result throughout the domain of interest will be recovered. The small divergence parameter β^2 was also introduced by Buchwald (1977) in the study of the effect of an irregular coastline. The depth profile $h(x,y)$ is assumed to be $h(x,y) = h_0(x) - \epsilon h_1(x,y)$ for a topographic irregularity $-\epsilon h_1(x,y)$ superimposed on the shelf zone, where $\epsilon = h_M/H_0 \ll 1$, h_M is the maximum height of the topographic irregularity, and h_0 the exponential profile of Buchwald and Adams (1968), i.e.,

$$h_0(x) = \begin{cases} e^{2b(x-1)}, & 0 \leqslant x \leqslant 1 \\ 1, & x \geqslant 1. \end{cases} \tag{2}$$

We also assume that Ψ can be expanded into a power series of order ϵ as follows:

$$\Psi(x,y,t) = \Psi_0(x,y,t) + \epsilon\Psi_1(x,y,t) + O(\epsilon^2). \tag{3}$$

Substituting (3) and the relation for $h(x,y)$ into (1) and equating like powers of ϵ, we obtain the $O(\epsilon^0)$ equation and related boundary conditions as follows:

$$\left.\begin{aligned} &\left(\Psi_{0xx} + \Psi_{0yy} - \frac{h_{0x}}{h_0}\Psi_{0x}\right)_t + \frac{h_{0x}}{h_0}\Psi_{0y} = 0, && 0 \leqslant x \leqslant 1 \\ &\Psi_{0xx} + \Psi_{0yy} - \beta^2\Psi_0 = 0, && x \geqslant 1 \\ &\Psi_0(x = 0, y, t) = \Psi_0(x \to \infty, y, t) = 0 \end{aligned}\right\}. \tag{4}$$

We further assume that the topographic irregularity is of a smooth type, i.e., if $l^{(x)}$, $l^{(y)}$ are length scales of h_1 in the x, y directions, respectively, then $\epsilon(l^{(x)})^{-1}$ and $\epsilon(l^{(y)})^{-1} \ll 1$.

The $O(\epsilon)$ equation and boundary conditions are

$$\left.\begin{aligned} &\left(\Psi_{1xx} + \Psi_{1yy} - \frac{h_{0x}}{h_0}\Psi_{1x}\right)_t + \frac{h_{0x}}{h_0}\Psi_{1y} \\ &\qquad = -\frac{h_{1y}}{h_0}(\Psi_{0yt} + \Psi_{0x}) + \left(\frac{h_{0x}}{h_0}\frac{h_1}{h_0} - \frac{h_{1x}}{h_0}\right)(\Psi_{0xt} - \Psi_{0y}), && 0 \leqslant x \leqslant 1 \\ &\Psi_{1xx} + \Psi_{1yy} - \beta^2\Psi_1 = 0, && x \geqslant 1 \\ &\Psi_1(x = 0) = \Psi_1(x \to \infty) = 0 \end{aligned}\right\}. \tag{5}$$

These equations hold for a topographic irregularity $[h_1(x,y) = h_1'(x,y)/h_M]$ confined to the shelf and slope region. Assuming that $\beta^2 \to 0$, then the O(1) equation and boundary conditions (4) for Ψ_0 are those for the free shelf waves considered by Buchwald and Adams (1968). The dispersion curves for $b = 1$ and $b = 2$ are shown in Fig. 1.

Assume that O(1) solution consists of only a free incident long wave with a group velocity to the south in the same direction as its phase speed, which is given by

$$\Psi_0 = \phi_0(x)e^{i(k_0y - \omega t)}, \tag{6}$$

where

$$\phi_0(x) = \begin{cases} e^{bx}\sin M_0 x, & 0 \leqslant x \leqslant 1, \\ e^{b}\sin M_0 \exp[-(\beta^2 + k_0^2)^{1/2}(x-1)], & x \geqslant 1, \end{cases} \tag{7}$$

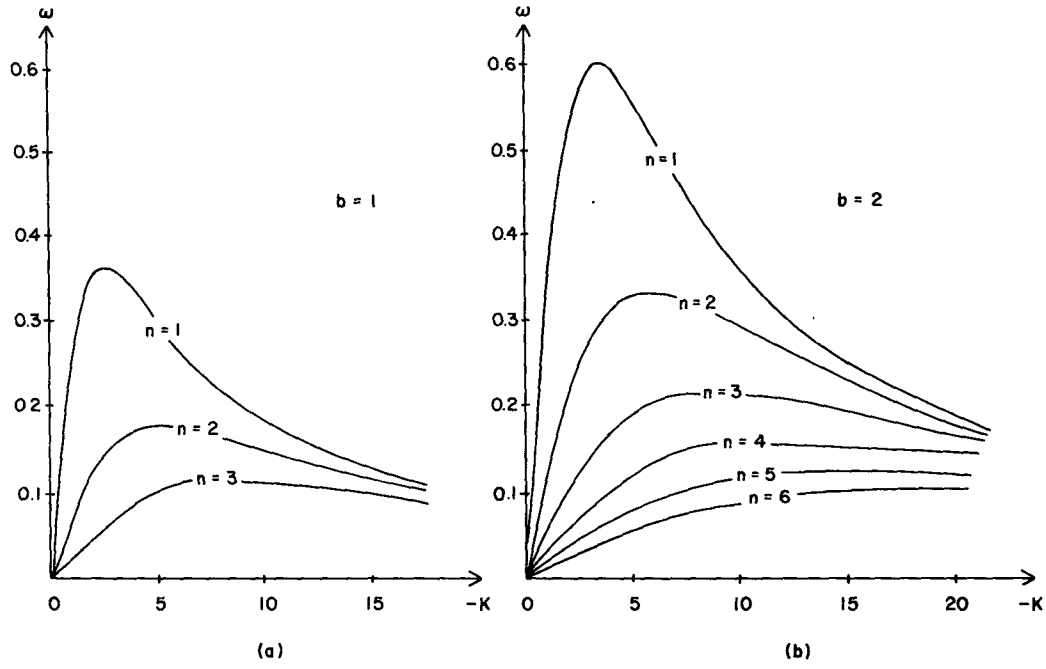

FIG. 1. Dispersion curves for (a) $b = 1$, (b) $b = 2$.

and $M_0 = (-k_0^2 - b^2 - 2bk_0/\omega)^{1/2}$. As can be seen from (7), ϕ_0 and ϕ_{ox} are continuous across $x = 1$, which is required for the continuity of onshore mass flux and pressure and for the free wave to be bounded in the Northern Hemisphere. For consistency we choose $\omega > 0$ and $k_0 < 0$.

To solve Eq. (5), we first take a Fourier transform in the longshore direction and apply a Green's function technique in the offshore direction. This method has been used by Chao and Janowitz (1978) in a study of horizontally sheared flow over an isolated topography. We next define the Fourier transforms

$$\begin{Bmatrix} \phi(x,k) \\ S(x,k) \end{Bmatrix} e^{-i\omega t} = \frac{1}{\sqrt{2\pi}} \int_{-\infty}^{+\infty} \begin{Bmatrix} \Psi_1(x,y,t) \\ R(x,y,t) \end{Bmatrix} e^{-iky} dy, \tag{8}$$

where $R(x,y,t)$ is the right-hand side of (5). We then have the following governing ordinary differential equations for ϕ:

$$\left.\begin{aligned} &\phi_{xx} - \frac{h_{0x}}{h_0}\phi_x - \left(k^2 + \frac{h_{0x}}{h_0}\frac{k}{\omega}\right)\phi = S/\omega, && 0 \leqslant x \leqslant 1 \\ &\phi_{xx} - (\beta^2 + k^2)\phi = 0, && x \geqslant 1 \end{aligned}\right\}. \tag{9}$$

The solution of (9) can be expressed as

$$\begin{aligned} \phi(x,k) &= \int_0^\infty G(x,\zeta;k)\frac{S(\zeta,k)}{\omega}\,d\zeta, \\ \Psi_1 &= \frac{1}{\sqrt{2\pi}} \int_{-\infty}^{+\infty} e^{i(ky-\omega t)} \left\{ \int_0^\infty G(x,\zeta;k)\frac{S(\zeta,k)}{\omega}\,d\zeta \right\} dk, \end{aligned} \tag{10}$$

where $G(x,\zeta;k)$ is the Green's function of (9) and can be written as

$$G(x,\zeta;k) = \begin{cases} \dfrac{\phi_1(x,k)\phi_2(\zeta,k)}{h_0(\zeta)D(k,\omega)}, & 0 \leqslant x < \zeta \\ \dfrac{\phi_1(\zeta,k)\phi_2(x,k)}{h_0(\zeta)D(k,\omega)}, & 0 \leqslant \zeta < x. \end{cases} \tag{11}$$

The functions $\phi_1(x,k)$ and $\phi_2(x,k)$ are the two homogenous solutions of (9), such that $\phi_1(0,k) = \phi_2(\infty,k) = 0$, and the Wronskian $h_0D(k,\omega)$ can be expressed as

$$h_0(x)D(k,\omega) = \phi_1\phi_{2x} - \phi_2\phi_{1x}.$$

In the particular case when $D(k,\omega) = 0$, for some (k,ω), the Wronskian becomes zero, $\phi_1 \propto \phi_2$, and ϕ_1 and ϕ_2 both satisfy the boundary conditions at $x = 0$ and $x \to \infty$ and thus become eigenfunctions of the homogeneous part of (9). Therefore, $D(k,\omega) = 0$ is the dispersion relation of which the real zeroes (k_n) of $D(k,\omega)$ yield the free wave solution of Buchwald and Adams.

It is straightforward to find ϕ_1 as

$$\phi_1 = \begin{cases} e^{bx}\sin Mx, & 0 \leq x \leq 1 \\ a_+ \exp[(\beta^2 + k^2)^{1/2}x] + a_- \exp[-(\beta^2 + k^2)^{1/2}x], & x \geq 1, \end{cases} \tag{12}$$

where $M = (-k^2 - b^2 - 2bk/\omega)^{1/2}$, and a_+, a_- can be found by requiring ϕ_1 and ϕ_{1x} continuous across $x = 1$. It follows that

$$a_\pm = \tfrac{1}{2}\exp[b \mp (\beta^2 + k^2)^{1/2}]\left[\sin M \pm \frac{b\sin M + M\cos M}{(\beta^2 + k^2)^{1/2}}\right]. \tag{13}$$

Similarly,

$$\phi_2 = \begin{cases} e^{bx}(b_+\sin Mx + b_-\cos Mx), & 0 \leq x \leq 1 \\ \exp[-(\beta^2 + k^2)^{1/2}x], & x \geq 1, \end{cases} \tag{14}$$

where

$$\left.\begin{aligned} b_+ &= \exp[-b - (\beta^2 + k^2)^{1/2}]\{-[b + (\beta^2 + k^2)^{1/2}]\cos M + M\sin M\}/M \\ b_- &= \exp[-b - (\beta^2 + k^2)^{1/2}]\{[b + (\beta^2 + k^2)^{1/2}]\sin M + M\cos M\}/M \end{aligned}\right\}. \tag{15}$$

Further, it is obvious that

$$D(k,\omega) = -\exp[b - (\beta^2 + k^2)^{1/2}][(b\sin M + M\cos M) + (\beta^2 + k^2)^{1/2}\sin M]. \tag{16}$$

The $O(\epsilon)$ streamfunction Ψ_1 can then be expressed as

$$\Psi_1(x,y,t) = \frac{1}{\sqrt{2\pi}}\int_{-\infty}^{+\infty}\int_0^\infty G(x,\zeta;k)\frac{S(\zeta,k)}{\omega}d\zeta e^{i(ky-\omega t)}dk. \tag{17}$$

The integral with respect to k is completed by considering k to be a complex variable. The integration along the real k axis is computed via a residue type calculation. It can be seen from relations (11)–(16) that the integrand of (17) is an even function of m and, therefore, branch cuts of (17) in the k plane come only from $(\beta^2 + k^2)^{1/2}$. We take the branch k to be the one for which $k \sim |k|$, as $k \to \infty$, so that the cuts are from $i\beta$ to $i\infty$, and from $-i\beta$ to $-\infty$.

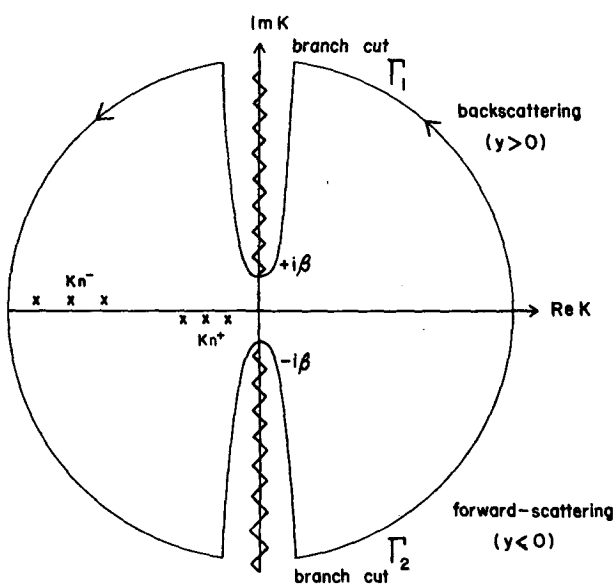

FIG. 2. Contours of integration for forward scattering ($y < 0$) and backscattering ($y > 0$).

The real zeroes (k_n) of $D(k,\omega)$ yield a wavelike part of Ψ_1 in (17). Complex zeroes of $D(k,\omega)$ and the contribution due to an integration about the branch cuts give solutions decaying in y, which are of no concern here and will not be computed. In compliance with the radiation condition we can include a small positive imaginary part of ω, i.e., $\omega = \omega_0 + i\sigma$. The effect of σ can be interpreted either as a frictional effect (see, e.g., Noble, 1958), or a slow turning-on of the forcing term (Lighthill, 1965). Once the small σ is included, all the k_n's with positive group velocity $(C_g^n = d\omega/dk\big|_{k=k_n^-} > 0)$ are shifted to the upper half k-plane, those k_n's with negative group velocity $(C_g^n = d\omega/dk\big|_{k=k_n^+} < 0)$ will be shifted to the lower half k-plane. The presence of e^{iky} in (17) suggests that one should close the contour of integration in the upper half k-plane for $y > 0$ (backscattering), and in the lower half k-plane for $y < 0$ (forward scattering). Fig. 2 illustrates the contours of integration for (17).

For large distances away from the bump ($|y| \gg 1$), the decaying solutions vanish and only wave-like solutions are taken into consideration; we then let $\sigma \to 0$, $\beta \to 0$. It can be seen that for all k_n such that $D(k,\omega) = 0$, $\phi_2 = b_+\phi_1$. Eq. (17) can be reduced to

$$\Psi_1^{\pm}(x,y,t) = \mp\sqrt{2\pi i}\sum_n \int_0^{\infty}\left[\frac{b_+(k)}{\partial D/\partial k}\frac{\phi_1(\zeta,k)}{h_0(\zeta)}\frac{S(\zeta,k)}{\omega}\right]_{k=k_n^{\pm}} d\zeta \times \phi_1(x,k_n^{\pm})\exp[i(k_n^{\pm}y - \omega t)], \quad |y| \gg 1, \quad (18)$$

for all possible k_n, where the + and − represent solutions for $y < 0$ and $y > 0$, respectively. It is simpler and conceptually useful to consider only a delta function bump, i.e., keep the dimensional volume of the bump V_b' fixed but shrink the size of the bump to zero, so that

$$\epsilon h_1(x,y) = \frac{V_b'}{H_0L^2}\delta(x - x_0)\delta(y). \quad (19)$$

The actual wave pattern over a realistic bump can be found by integrating the delta-function solution over an extended topography. Eq. (18) can then be further reduced to

$$\epsilon\Psi_1^{\pm}(x,y,t) = \mp\frac{iV_b'}{H_0L^2}\sum_{n=1}^{N}\left\{\frac{b_+(k)}{\partial D/\partial k}\frac{1}{\omega h_0^2}\times[k(\omega k_0\phi_0 + \phi_{0x})\phi_1 + (\omega\phi_{0x} + k\phi_0)\phi_{1x}]\right\}_{\substack{k=k_n^{\pm}\\ x=x_0}} \times \phi_1(x,k_n^{\pm})\exp[i(k_n^{\pm}y - \omega t)], \quad (20)$$

where upper and lower signs represents forward scattering ($y < 0$) and backscattering ($y > 0$), respectively. The term in braces gives the amplitude ($A_n^{\pm}$) of the scattered waves. We can see that if $D(k,\omega(k)) = 0$ is considered as the dispersion relation, then

$$dD = \left(\frac{\partial D}{\partial k} + \frac{\partial D}{\partial\omega}\frac{d\omega}{dk}\right)dk = 0$$

and

$$\frac{\partial D}{\partial k}(k_n,\omega) = -\frac{\partial D}{\partial\omega}C_g^n. \quad (21)$$

It is immediately seen from (20) and (21) that, if the incident shelf wave has frequency ω at which there is a ZGS in the highest possible mode, resonance then occurs, consistent with the result of Buchwald (1977). The implication of this resonance is that there is a bandwidth $\Delta\omega \sim O(\epsilon^2)$ around each ZGS for which the amplitudes of diffracted waves are nearly of the same size as the incident wave (Buchwald, 1977). We can also see from (20) that the scattered wave (Ψ_1) is ±90° out of phase with the incoming wave Ψ_0.

3. Numerical results

Fig. 3 shows the amplitudes of the backscattered (A_n^-) and forward-scattered (A_n^+) waves versus the location of the bump which varies from $x_0 = 0$ to $x_0 = 1$ for a first-mode, long incident wave with $b = 1$ and $\omega = 0.1$. It is interesting to see that for a first-mode incident wave scattered into the nth mode, there are $n + 1$ nodal points of $A_n^{\pm}$ at which an isolated bump does not generate scattered waves

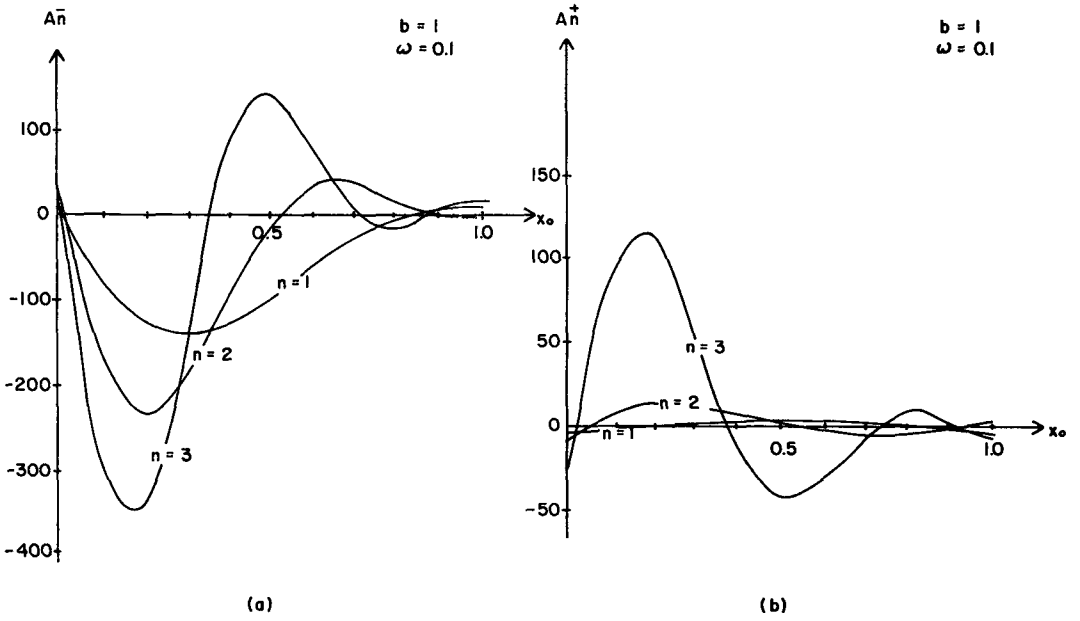

FIG. 3. Amplitudes of (a) backscattered, and (b) forward-scattered shelf waves versus the location of the bump (x_0) for a first-mode, long incident wave with $b = 1$, $\omega = 0.1$.

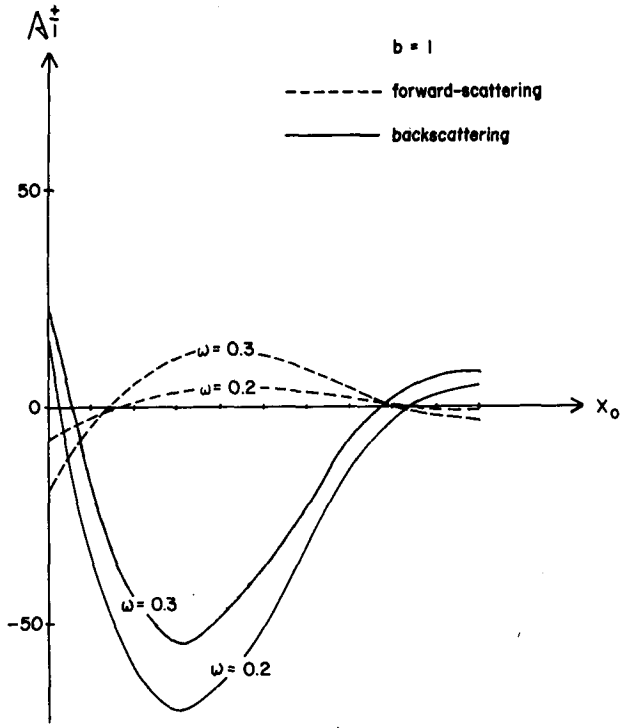

FIG. 4. Amplitudes of forward-scattered (dashed line) and backscattered (solid line) waves versus χ_0 for a first-mode, long incident wave with $b = 1$; $\omega = 0.2$, 0.3. Only first-mode wave is possible.

at all. The amplitude of scattered waves for a nearshore bump tends to be larger than that for an offshore bump. In general, that is, for most values of x_0 the amplitude is the largest for $n = 3$ mode and the smallest for $n = 1$. Thus a long shelf wave is likely to be scattered by an isolated bump into the highest mode. It is also true that backscattered waves are more intense than forward-scattered waves.

Fig. 4 shows $A_n^{\pm}$ vs x_0 for a first-mode, long incident wave with $b = 1$, $\omega = 0.2$ and 0.3. As can be seen from Fig. 1, only first-mode waves exist at these higher frequencies. Comparisons can only be made for the first-mode waves. A combination of Figs. 3 and 4 shows that for the first-mode scattered waves, the higher the frequency of the incident wave, the higher the amplitude of the forward-scattered wave and the lower the amplitude of the backscattered wave.

Fig. 5 shows the amplitude ($A_n^{\pm}$) vs x_0 for a first-mode, long incoming wave with $b = 2$, $\omega = 0.2$. The figure indicates essentially the same trend as in Fig. 3. In addition, the effect of a larger b is in general to produce larger amplitudes of both forward-scattered and backscattered waves for the same mode and frequency. We also computed $A_n^{\mp}$ at higher frequencies for $b = 2$. Results show a similar behavior to those in Fig. 4, and hence are not presented here.

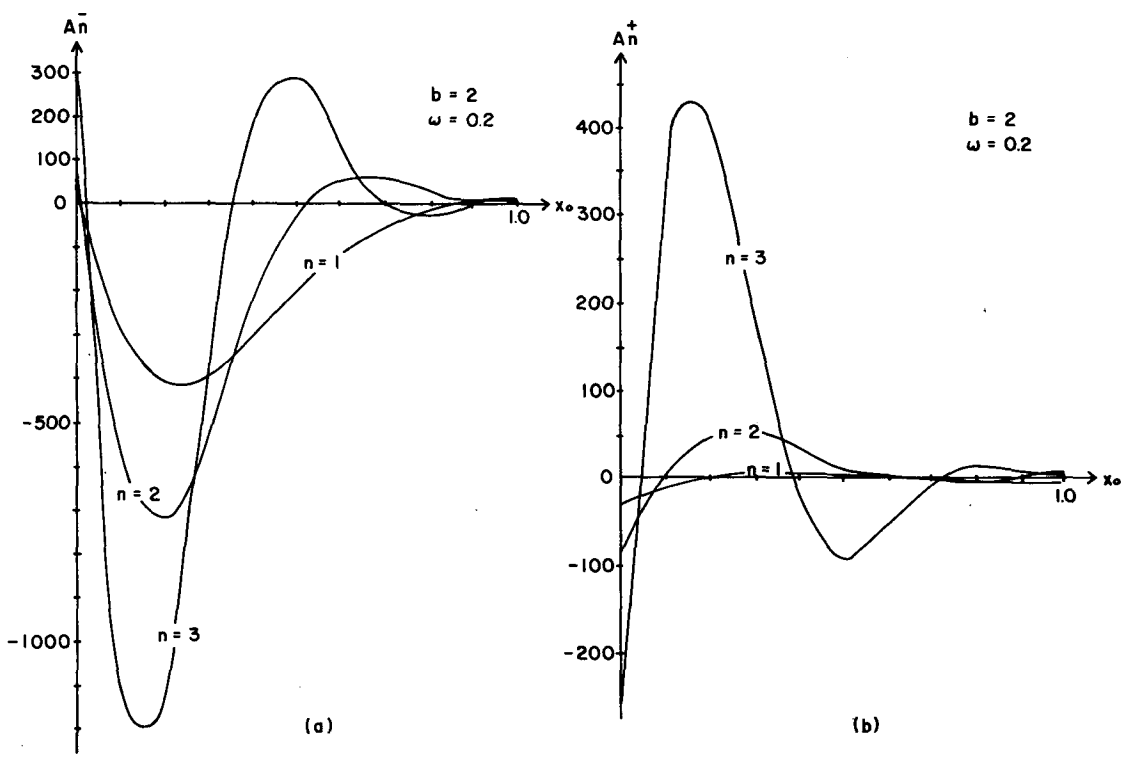

FIG. 5. Amplitudes of (a) backscattered, (b) forward-scattered shelf waves versus χ_0 for a first mode, long incident wave with $b = 2$, $\omega = 0.2$.

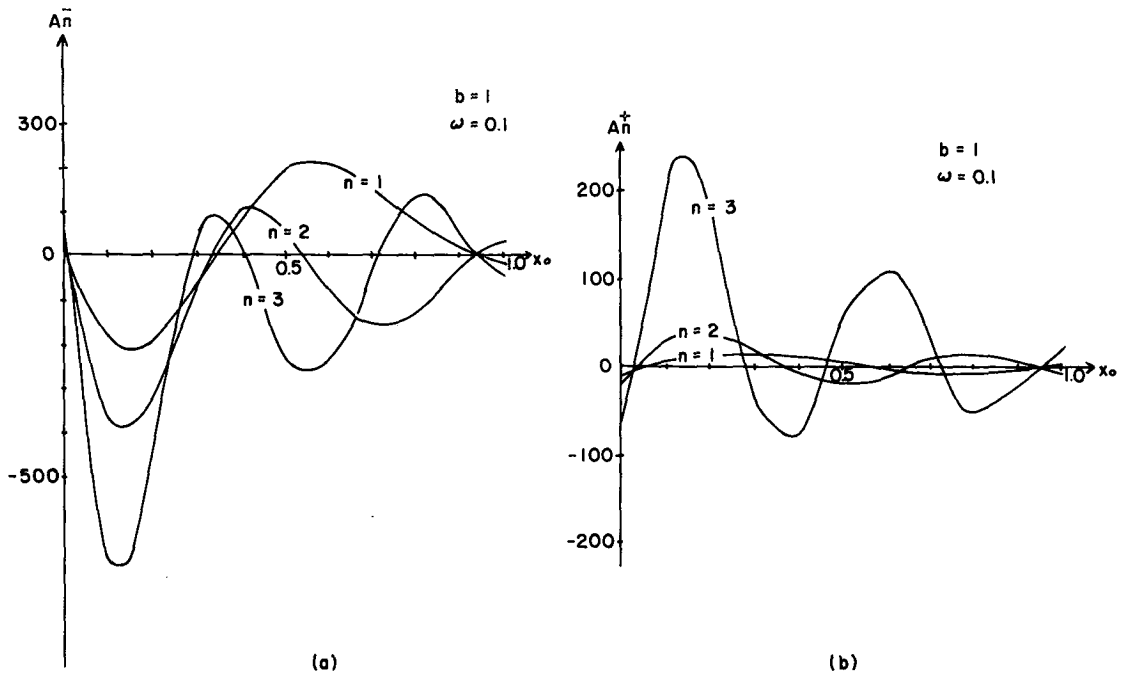

FIG. 6. As in Fig. 3 except for a second-mode, long incident wave with $b = 1$, $\omega = 0.1$.

Figs. 6 and 7 show the wave amplitude versus x_0 for second-mode ($m = 2$) and third-mode ($m = 3$), long incident waves, respectively, for $b = 1$ and $\omega = 0.1$. There are $n + m$ nodal points of $A_n^{\pm}$ for an mth mode wave scattered into an nth mode wave as expected. Combining with Fig. 3, one can see that, in general, the highest mode incoming wave has the strongest tendency to be scattered by an isolated bump. For a first-mode incoming wave, the largest amplitude peak of scattered waves usually occurs for $x_0 < 0.2$ and as x_0 gets larger, subsequent peaks decay rather quickly. This

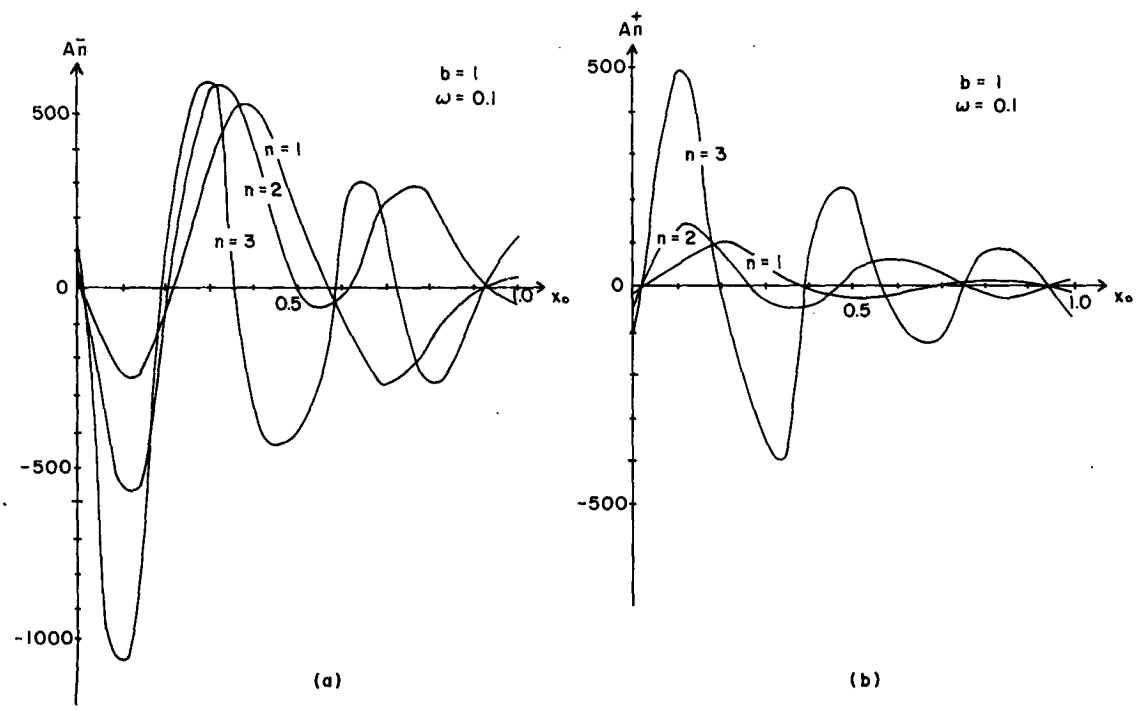

FIG. 7. As in Fig. 3 except for a third-mode, long incident wave with $b = 1$, $\omega = 0.1$.

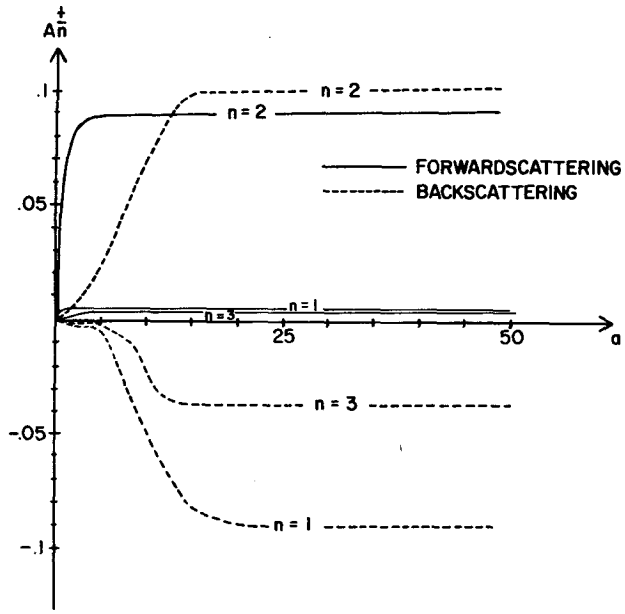

FIG. 8. The scattered amplitudes ($A_n^{\pm}$) for an extended topographic irregularity [Eq. (25)] for $b = 1$, $\omega = 0.1$.

last statement remains true for the forward-scattered waves of a higher mode incoming wave. However, the situation becomes quite different when we consider backscattered waves. As the incident mode becomes higher and as x_0 increases, successive amplitude peaks decays more slowly. Furthermore, other than the first amplitude peak ($x_0 < 0.2$), incident wave energy is more evenly scattered into all possible modes for a higher incoming mode. The implication is that as far as the backscattering is concerned, an offshore bump becomes more effective for a higher, incoming mode and higher scattered modes. However, it is always true that the forward-scattering and backscattering processes favor the highest mode because C_g^3, and hence $\partial D/\partial k$ for $n = 3$, is the smallest. In the case of a third-mode incident wave, A_3^- is only slightly favored for $x_0 > 0.2$ as shown in Fig. 7a.

The model developed in Section 2 essentially deals with a small and smooth topographic irregularity with a delta-function bump having been used to complete the analysis. The validity of extending the delta-function results to the smooth bump case will now be addressed. Note that for a delta function located at point x_0, y_0, the Green's function solution for the streamfunction can be written as

$$\Psi_g(x,x_0,y,y_0) = \sum_n V_b'(x_0,y_0)B(x_0,k_n)\phi_1(x,k_n) \times \exp\{i[k_m(y - y_0) - \omega t]\}. \quad (22)$$

For a small and smooth bump of horizontal extent $l^{(x)}$ and $l^{(y)}$ in the x and y directions, respectively, $\epsilon\Psi_1$ can be obtained by integrating (22) over the extended topographic irregularity, i.e.,

$$\epsilon\Psi_1(x,y,t) = \int_{l^{(x)}} dx_0 \int_{l^{(y)}} dy_0 \Psi_g(x,x_0,y,y_0). \quad (23)$$

It can be seen from (23) that if $k_n l^{(y)} \ll 1$ and $l^{(x)}\ \mathrm{Max}\{M_0,M\} \ll 1$, then all of the variables save for $V_b'(x_0,y_0)$ can be legitimately removed from within the double integral, so that the delta-function solution given by (20) is approximately applicable. For the delta-function solution to be more than approximately valid, it is required that the inequalities expressed as

$$\left.\begin{aligned} &\mathrm{Min}\{M_0^{-1},M^{-1}\} \gg l^{(x)} \gg \epsilon \\ &k_n^{-1} \gg l^{(y)} \gg \epsilon \end{aligned}\right\} \quad (24)$$

be satisfied. As the bump widens, cancellation of waves occurs over point pairs on the bump and the delta-function results begins to gradually lose meaning.

It is noted that the amplitudes of scattered waves can be different from those depicted by the Green's function solution if an extended topographic irregularity were considered. For example, we consider the effect of a topographic ridge described by the expression

$$\epsilon h_1(x,y) = \frac{a}{10\pi\sqrt{2}} \exp[-a^2y^2 + 2b(x - 2)] \times \sin\pi x, \quad 0 \leq x \leq 1. \quad (25)$$

The ridge extends from $x = 0$ to $x = 1$ and is Gaussian in the alongshore direction. The parameter a is inversely proportional to the alongshore scale of the bump, i.e., $a \propto (l^{(y)})^{-1}$. The volume of the bump remains fixed throughout. Invoking relation (23) to compute the amplitudes of forward and backward scattered waves, A_n^+ and A_n^-, for $b = 1$, $\omega = 0.1$ leads to the results depicted in Fig. 8. From the result it is obvious that as the alongshore scale of the bump is diminished, the magnitudes of the scattered wave amplitudes approach those which result from imposing a delta-function bump in y, i.e., $\delta(y)$. For an increase in wavenumber of a scattered wave, it is required that $l^{(y)}$ or a^{-1} be correspondingly diminished, consistent with relation (24), in order that a delta-function solution be approached. The secondary backscattered wave mode, represented by A_2^-, has greatest amplitude when the alongshore structure of the ridge approaches a delta function. If the size of the bump is reduced in the cross-shelf direction sufficient to justify the condition that $l^{(x)} \ll 1$, then the results depicted in Fig. 3 may once again be applied.

4. Conclusions

We briefly summarize what has been accomplished in this paper. For an incoming, long CSW over a

small smooth bump of small $l^{(x,y)}$ superimposed on an exponential shelf:

1) The amplitudes of scattered waves are in general a function of the offshore location of the bump, and are larger for a bump nearer to the shore.

2) The scattering process always favors the higher incoming mode and higher scattered mode.

3) An offshore bump ($x_0 > 0.2$ in general) backscatters a higher incoming mode wave more effectively and more evenly into all possible modes.

4) Backscattered shelf waves are in general more intense than forward-scattered shelf waves, but a higher frequency incident wave will strengthen the forward scattering and weaken the backscattering, thus making the scattering process more "longshorely isotropic."

5) The effect of a larger b is in general to produce larger amplitudes of scattered waves.

6) The scattered shelf waves are $\pm 90°$ out of phase with the incident wave.

7) There are $n + m$ nodes where the bump does not scatter waves for an mth mode incoming wave scattered into an nth mode.

A long shelf wave propagating along a complicated and extended longshore topography is more likely to be scattered into the highest possible mode, which in turn has the strongest tendency to be scattered, but still favors the higher modes. Therefore, we would expect that eventually some of the wave energy will be transferred to higher wavenumber shelf waves. If we have a continuous spectrum of long shelf waves incident on an extended topography, there will be a net cascading process which transfers the low-wavenumber spectrum into a higher wavenumber spectrum due to topographic effects alone.

In the case of an "extended" topographic irregularity, relation (23) can be used to compute the amplitudes of the scattered waves and these amplitudes can, and most likely will, vary as the irregularity is increased in size.

The model developed herein can be further generalized for arbitrary continental shelf and slope topography and melded with a flat bottom ocean interior region, with the operational constraint that ϕ_1 and $\partial D/\partial k$ in relation (20) must be evaluated numerically for all allowable k_n's.

Acknowledgments. We thank Mr. W. C. Liou for his assistance in programming and to Mrs. Toni Clay for drafting the figures. This research was sponsored by U.S. Department of Energy under Contract EY-76-S-09-0902, and by the National Science Foundation under Grant ATM76-15871.

REFERENCES

Allen, J. S., 1976: Continental shelf waves and alongshore variations in bottom topography and coastline. *J. Phys. Oceanogr.*, **6**, 864–878.

Buchwald, V. T., 1977: The diffraction of shelf waves by small coastal irregularities. *Proc. IUTAM Symp. Waves on Water of Variable Depth*, Canberra, *Lecture Notes in Physics*, Vol. 64, D. G. Probis and R. Radok, Eds., Australian Academy of Science, Spring-Verlag, 231 pp.

——, and J. K. Adams, 1968: The propagation of continental shelf waves. *Proc. Roy. Soc. London*, **A305** 235–250.

Chao, S. Y., and G. S. Janowitz, 1979: The effect of localized topographic irregularity on the flow of boundary current along the continental margin. *J. Phys. Oceanogr.*, **9** (in press).

Cutchin, D. L., and R. L. Smith, 1973: Continental shelf waves: Low frequency variations in sea level and currents over the Oregon continental shelf. *J. Phys. Oceanogr.*, **3**, 73–82.

Hamon, B. V., 1976: Generation of shelf waves on the east Australian coast by wind stress. *Memo. Soc. Roy. Sci. Liege*, **10**, 359–367.

Huthnance, J. M., 1975: On trapped waves over a continental shelf. *J. Fluid Mech.*, **67**, 689–704.

LeBlond, P. H., and L. A. Mysak, 1977: Trapped coastal waves and their role in shelf dynamics. *The Sea*, E. D. Goldberg, I. N. McCave, J. J. O'Brien and J. H. Steele, Eds., Vol. 6, Wiley-Interscience, 459–495.

Lighthill, M. J., 1965: Group velocity. *J. Inst. Math. Appl.*, **1**, 1–28.

Noble, B., 1958: *Methods Based on the Wiener-Hopf Technique*. Pergamon Press, 246 pp.

Odulo, A. B., 1975: Propagation of long waves in a rotating basin of variable depth. *Okeanologiya*, **15**, 11–15.